STATE OF THE CLIMATE IN 2008

T. C. Peterson and M. O. Baringer, Eds.

Associate Eds.: H. J. Diamond, R. L. Fogt, J. M. Levy, J. Richter-Menge, P. W. Thorne, L. A. Vincent, and A. B. Watkins

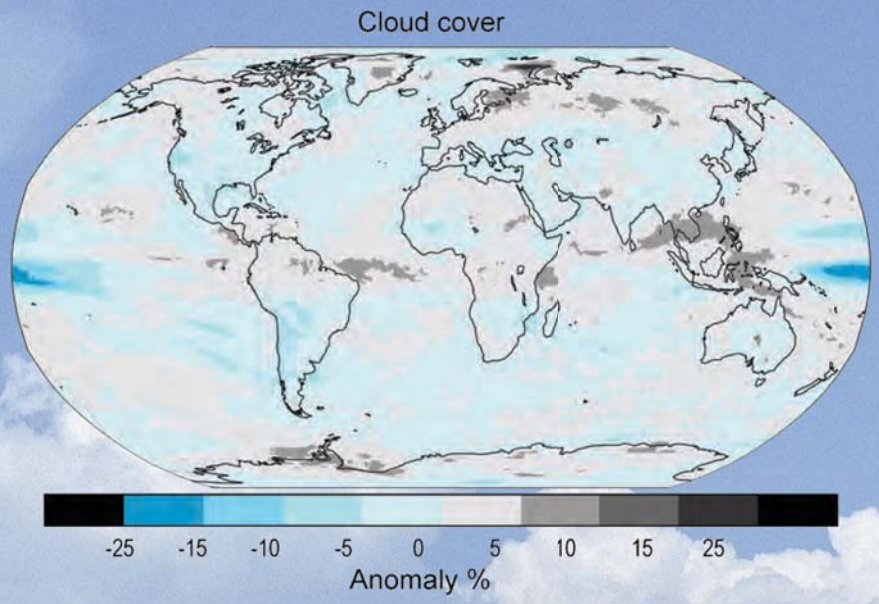

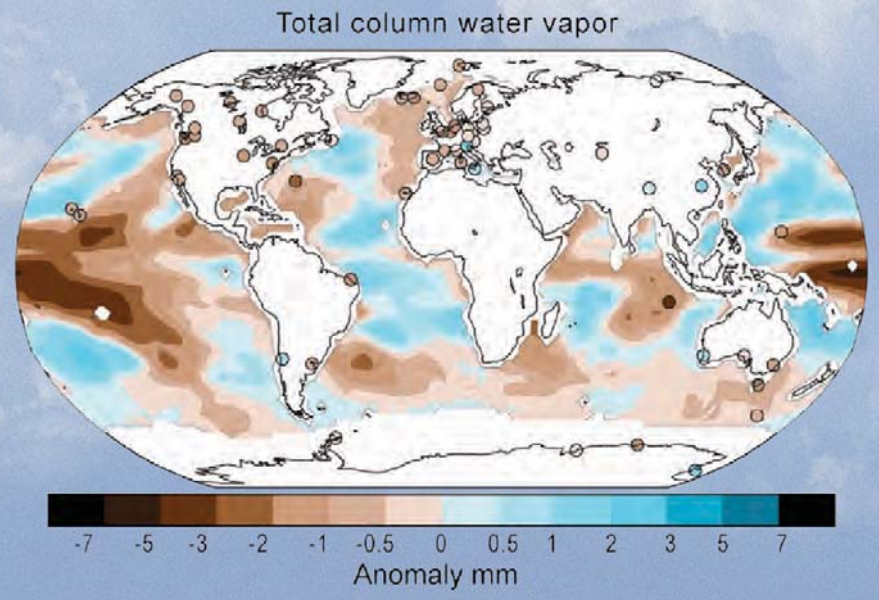

Special Supplement to the *Bulletin of the American Meteorological Society*
Vol. 90, No. 8, August 2009

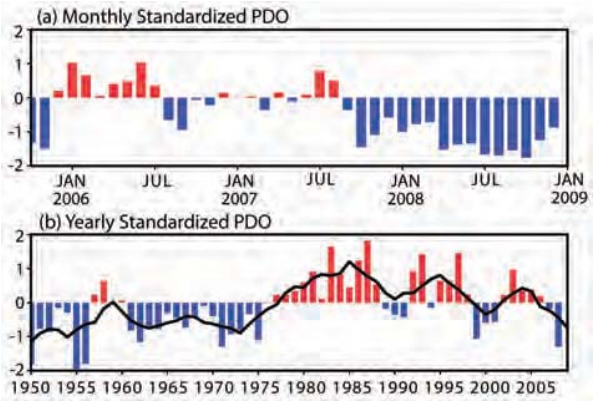

Fig. 3.3. (a) Monthly standardized PDO index (bar) in the past four years and (b) yearly mean of the monthly PDO index (bar) overlapped with the 5-yr running mean of the index (black line) in 1950–2008. The PDO index was downloaded from University of Washington at http://jisao.washington.edu/pdo.

persisted through calendar year 2008 (Fig. 3.3a). The longer-term yearly mean PDO index illustrates prominent low-frequency variability with a downward trend from the mid-1980s to the present (Fig. 3.3b). Interestingly, the PDO value in 2008 was the lowest since 1971. Along with the negative PDO phase, upwelling along the west coast of North America was also well above normal during the 2008 upwelling season, which favored high biological productivity during the past year (Frank Schwing 2009, personal communication).

The global mean SST in 2008 was slightly cooler than that in 2007 (Fig. 3.4a), largely due to the cooling in the central tropical Pacific, the Arctic Ocean, and the regions extending from the Gulf of Alaska to the west coast of North America (Fig. 3.2b). The 2008 minus 2007 SSTA differences largely resemble the negative PDO pattern, which is also reflected in the anomaly differences of surface latent plus sensible heat flux (Fig. 3.8b). The tripole SST pattern in the North Atlantic is also reflected in the heat fluxes.

The global mean SST in 2007 and 2008 was much cooler than that during 2002–06 (Fig. 3.4a). The cooling in the past two years was largely due to the cooling in the tropical Pacific (Fig. 3.4b), which is associated with the 2007–08 La Niña and persistent negative PDO (Fig. 3.3a). The cooling in the tropical Pacific contributed to the cooling in the global tropical oceans in the past two years, although the contributions from the tropical Indian and Atlantic Oceans were less evident (Figs. 3.4c–e). From a historical perspective, the global mean SST was below normal (1971–2000 average) during 1950–76 and has been persistently above normal since 1997. Although the global mean and tropical mean SSTAs all have a prominent upward trend from 1950 to 2008, similar trends are not evident in the North Pacific and North Atlantic (Figs. 3.4f–g).

c. Ocean heat content—G. C. Johnson, J. M. Lyman, J. K. Willis, S. Levitus, T. Boyer, J. Antonov, C. Schmid, and G. J. Goni

Storage and transport of heat in the ocean are central to aspects of climate such as El Niño (e.g., Zebiak 1989), the North Atlantic Oscillation (e.g., Curry

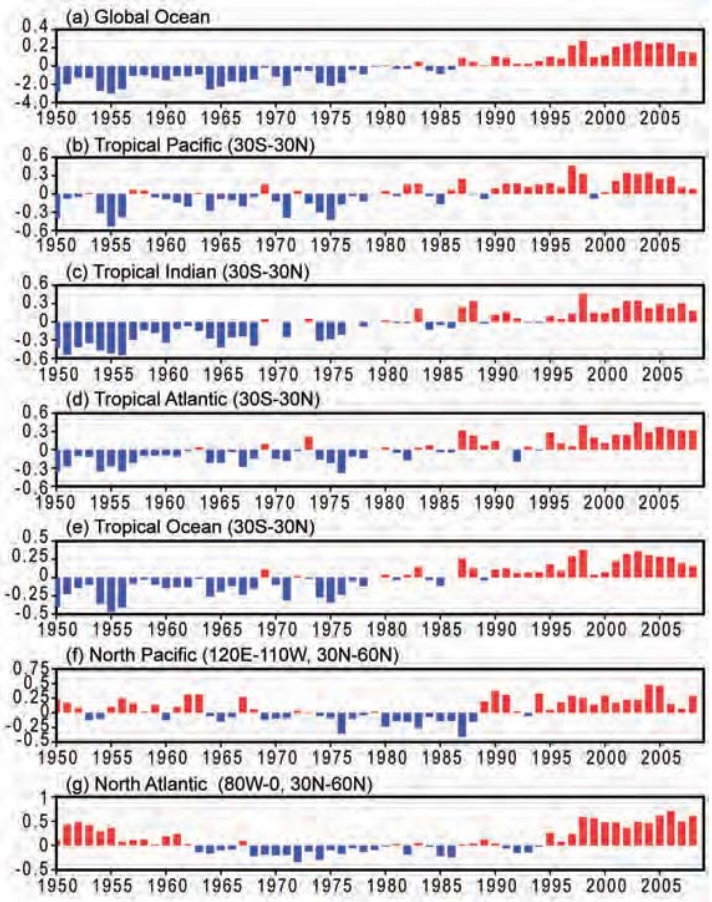

Fig. 3.4. Yearly mean SST anomalies (°C) averaged in (a) the global ocean, (b) tropical Pacific Ocean, (c) tropical Indian Ocean, (d) tropical Atlantic Ocean, (e) all three tropical oceans, (f) North Pacific, and (g) North Atlantic in 1950–2008. SSTs are the ERSST v.3b of Smith et al. (2008). All anomalies are defined as departures from the 1971–2000 climatology (Xue et al. 2003).

and McCartney 2001), hurricanes (e.g., Mainelli et al. 2008; Vecchi et al. 2008), sea level rise (e.g., Domingues et al. 2008), and global warming (e.g., Hansen et al. 2005).

We begin by discussing an estimate of upper (0–750 m) OHCA for the period 1 January–31 December 2008 (Fig. 3.5a) computed from a combination of in situ ocean temperature data and satellite altimetry data, following Willis et al. (2004) but relative to a 1993–2008 baseline, hereafter the combined estimate. We also discuss changes in the combined estimate between 2008 and 2007 (Fig. 3.5b). We contrast these combined estimate changes with changes of mixed layer OHCA (Fig. 3.6) derived from in situ observations (Schmid 2005), hereafter the mixed layer estimate. We also put the estimates of recent upper-OHCA variability into a longer-term context using a time series of global integrals of 0–700-m in situ OHCA from 1955 through 2008 (Fig. 3.7), a time period much longer than the satellite altimeter record, estimated following Levitus et al. (2009), hereafter the in situ estimate.

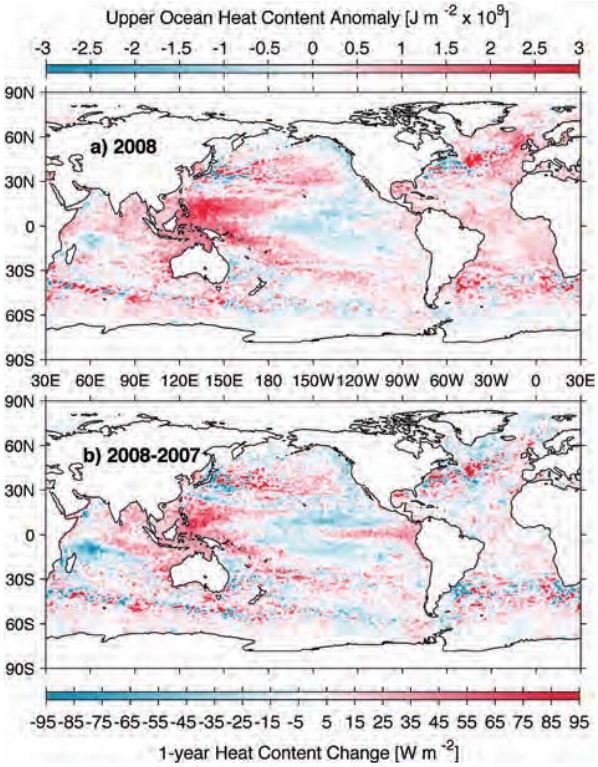

Fig. 3.5. (a) Combined satellite altimeter and in situ ocean temperature data estimate of upper- (0–750 m) ocean heat content anomaly OHCA (10^9 J m^{-2}) for 2008 analyzed following Willis et al. (2004) but relative to a 1993–2008 baseline. (b) The difference of 2008 and 2007 combined estimates of OHCA expressed as a local surface heat flux equivalent (W m^{-2}). For panel comparisons, note that 95 W m^{-2} applied over one year results in a 3 × 10^9 J m^{-2} change of OHCA.

In recent years many of the globally distributed in situ subsurface ocean temperature data are from Argo (Roemmich et al. 2004). Data from Argo floats with the potential for as yet uncorrected systematic pressure biases (www.argo.ucsd.edu/Acpres_drift_apex.html) have been removed from the combined estimate presented here. In addition, annual estimates of XBT fall-rate corrections have been applied for deep- and shallow-probe data following Wijffels et al. (2008) for the combined estimate, but with no XBT data used after 2005. A somewhat different set of corrections to MBTs and XBTs for all years is applied for the 0–700-m in situ estimate following Levitus et al. (2009). The mixed layer estimate uses Argo and GTSPP (www.nodc.noaa.gov/GTSPP/) data subject to Argo real-time quality-control criteria followed by local statistical checks to eliminate remaining outliers. Details of all the fields analyzed here may change after data from floats with potential pressure biases are corrected and made available, after more real-time data are subject to delayed-mode scientific quality control, and as XBT and MBT corrections improve.

The 2008 0–750-m combined estimate of OHCA (Fig. 3.5a) shows eddy and meander variability down to the 100-km mapping scales, as does, to a greater extent, the difference of the 2008 and 2007 combined estimates (Fig. 3.5b). Strong small-scale spatial variability in OHCA fields is associated with the western boundary currents in every gyre, as well as the Antarctic Circumpolar Current. The difference in combined estimates between 2008 and 2007 (Fig. 3.5b) illustrates the large year-to-year variability in ocean heat storage, with changes reaching or exceeding the equivalent of a 95 W m^{-2} magnitude surface flux applied over one year (~3 × 10^9 J m^{-2}). Ocean advection likely plays a significant role in many of these changes. Upper OHCA, deep variability, freshwater, and mass signals all contribute to sea level anomalies. Despite this, there are many large-scale visual similarities between upper-OHCA (Fig. 3.5) and sea level (Fig. 3.21) fields in 2008, even relative to their differing baseline periods.

Large-scale patterns are evident in OHCA for 2008 (Fig. 3.5a) and its difference from 2007 (Fig. 3.5b). The central equatorial Pacific is still low in heat content, as it was during 2007 due to a La Niña (Levinson and Lawrimore 2008), and the off-equatorial central and eastern tropical Pacific OHCA values also fell from 2007 to 2008. However, the eastern equatorial Pacific heat content has risen to values slightly above

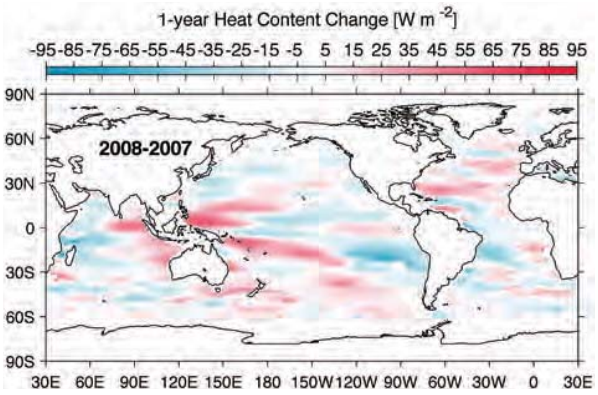

Fig. 3.6. Change of ocean mixed layer heat content estimated following Schmid (2005) expressed as a surface heat flux equivalent (W m^{-2}). The map is based on subtraction of a yearly mean of ocean mixed layer content for calendar year 2008 from that for calendar year 2007.

the mean in that interval, and the western tropical Pacific heat content has risen to levels well above the mean. While the annual averaging period presented here is too long for detailed study of the movement of heat associated with ENSO dynamics, certainly the change on the equator and perhaps those in the off-equatorial regions are related to those processes (e.g., Zebiak 1989).

Like the western tropical Pacific, the northeastern Indian Ocean continued gaining heat between 2007 and 2008 (Fig. 3.5b), as both regions did between 2006 and 2007 (Levinson and Lawrimore 2008). As a result, OHCA in the northeastern Indian Ocean in 2008 is above the mean (Fig. 3.5a), contrasting clearly with below-average values found in 2006 (Aguez et al. 2007). Around 10°S in the Indian Ocean heat was lost in the western half and gained in the east from 2007 to 2008 (Fig. 3.5b), largely the reverse of the tendency in this region from 2006 to 2007 (Levinson and Lawrimore 2008), leaving the area around the Seychelles slightly below the mean for OHCA in 2008 (Fig. 3.5a).

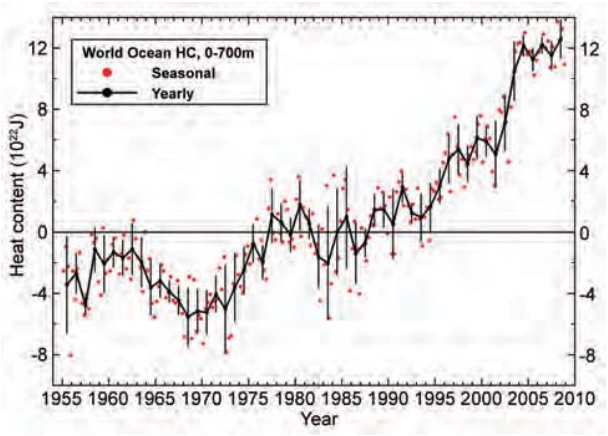

Fig. 3.7. Time series of quarterly (red dots) and annual average (black line) global integrals of in situ estimates of upper OHCA (10^{22} J) for the 0–700-m layer from 1955 to 2008, following Levitus et al. (2009). Error bars for the annual values are 1 std dev of the four quarterly estimates in each year. Additional error sources include sampling errors (Lyman and Johnson 2008) and remaining uncorrected instrument biases (Levitus et al. 2009).

The North Pacific shows high OHCA in its center in 2008, and low OHCA off the west coast of North America (Fig. 3.5a). This pattern is consonant with a strongly negative Pacific decadal oscillation (Mantua et al. 1997) during 2008, and hence mirrored in sea surface temperature anomalies for 2008 (Fig. 3.2). The band of high OHCA near 35°S in the South Pacific (Fig. 3.5a) appears to have steadily migrated south from lower subtropical latitudes in 2007 (Fig. 3.5b), and even lower tropical latitudes in 2006 (Aguez et al. 2007).

In the subpolar North Atlantic, the Labrador and Irminger Seas cooled between 2007 and 2008 (Fig. 3.5b), returning OHCA values in these areas to near the 1993–2008 mean (Fig. 3.5a), consonant with a return of deep wintertime convection there in early 2008 (Våge et al. 2009). A strong warming centered near 45°N, 45°W (Fig. 3.5b) suggests a local northwestward shift in the North Atlantic Current in 2008 relative to the previous year. The continued high OHCA values in the eastern subpolar North Atlantic (Fig. 3.5a) suggest that subtropical influences are still strong there, consistent with anomalously salty surface conditions in that region in 2008 (Fig. 3.13). The subtropical and tropical Atlantic in both hemispheres remains slightly warmer than the mean, with little change from 2007 to 2008.

Near the Antarctic Circumpolar Current, OHCA is highly variable (Fig. 3.5a) and appears anomalously cool in the Pacific, warm in the Indian, and mixed in the Atlantic in 2008, a less coherent pattern than in the previous few years (Arguez et al. 2007; Levinson and Lawrimore 2008). This lack of coherence may be related to a shift in the Antarctic Oscillation Index to positive in 2008, after several years of negative values.

A map of year-to-year changes in mixed layer OHCA (Fig. 3.6) shows many similarities to the map of 2008–07 0–750-m combined OHCA (Fig. 3.5b). However, the figures are not directly comparable. The mixed layer map (Fig. 3.6) is much smoother than the analogous combined OHCA map (Fig. 3.5b) because

the former map uses much longer decorrelation length scales (20° lon and 4° lat) than the latter. The difference in scales arises because the combined maps of 0–750-m OHCA use altimeter data to increase resolution and fill in where in situ data are sparse.

These methodological differences notwithstanding, the magnitudes of year-to-year changes in the mixed layer (Fig. 3.6) are generally smaller than those from the combined estimates for 0–750 m (Fig. 3.5b). This reduction in magnitude is expected because year-to-year OHCA changes can extend below the mixed layer. In addition, there are a few regions with qualitative differences in the two quantities, such as on either coast of South America around 20°S, where the mixed layer heat content anomaly has fallen over the course of a year (Fig. 3.6), but there is no such change evident in the combined map of upper OHCA (Fig. 3.5b). Changes in mixed layer depth can have large impacts on the heat content in the mixed layer even if there is no change in the mixed layer temperature, and that fact could be the reason for such striking differences.

Over a multidecadal period, upper-ocean estimates (0–700 m) of in situ ocean heat content following Levitus et al. (2009) reveal a large increase in global integrals of that quantity (Fig. 3.7). Global integrals of the in situ estimates for the last several years have reached consistently higher values than for all prior times in the record. The recent several-year plateau has smaller variability than the rest of the record, probably because of the effects of the excellent data coverage (Lyman and Johnson 2008) as provided by Argo floats (Roemmich et al. 2004). However, there are also long stretches in the record prior to 2000 that also exhibit little upward trend in OHCA.

Finally, around Antarctica and in the northern North Atlantic, near-surface water becomes dense enough to sink to the abyssal ocean, spreading around the globe (e.g., Lumpkin and Speer 2007). The ocean below the 2-km target depth for Argo profiles is not frequently sampled, making quantitative annual global estimates of abyssal ocean heat content changes impossible. However, there is observational evidence that the deep oceans, including the North Atlantic, have gained heat at least to 3,000 m over the past few decades (Levitus et al. 2005). Furthermore, analyses of recent repeated hydrographic observations in the deep South Atlantic (Johnson and Doney 2006), Pacific (Johnson et al. 2007), and South Indian Oceans (Johnson et al. 2008a) suggest that Antarctic Bottom Water has warmed over the last decade and that this warming could make a contribution to the global heat budget on the order of 10%–20%.

d. Global ocean heat fluxes—L. Yu and R. A. Weller

Much of the solar energy absorbed at the top ocean layer is released back to the atmosphere by two heat exchange processes at the air–sea interface: evaporation that releases latent heat and conduction and convection that releases sensible heat. These air–sea heat exchanges cool the ocean but warm the air, supplying the heat energy needed to drive the atmospheric circulation and global weather patterns. Clearly, air–sea heat fluxes (i.e., the amount of air–sea heat exchange) are a key measure of the role that the ocean plays in global climate, and their changes on short-term and long-term time scales may have important climate implications.

The global distribution of latent and sensible heat fluxes in 2008 (Fig. 3.8a) shows that on an annual basis the largest ocean heat losses occur over the regions associated with major WBCs and their extensions (e.g., the Kuroshio off Japan, the Gulf Stream off the United States, and the Agulhas Current off the African coast). The magnitude of the annual mean LHF + SHF in these regions exceeds 250 W m^{-2}, produced largely during the fall-to-winter seasons by strong winds and cold and dry air masses coming from the land (Bigorre and Weller 2008). The second-largest heat loss (~180 W m^{-2}) is located over the broad subtropical southern Indian Ocean, where the large air–sea heat exchange is sustained primarily by the strong southeast trade winds in the monsoon months June–September.

The estimates of LHF + SHF were produced by the OAFlux project (Yu et al. 2008) at WHOI. The computation of the OAFlux products uses the state-of-the-art bulk flux algorithm version 3.0 by Fairall et al. (2003), with the surface meteorological variables determined from an optimal blending of satellite retrievals and atmospheric reanalysis/forecast models of NCEP and ECMWF. The accuracy of the OAFlux LHF and SHF estimates was evaluated using 105 buoys available over the global oceans (Yu et al. 2008, manuscript submitted to *J. Climate*). The averaged root-mean-square differences between OAFlux and buoy calculated over the buoy locations are 9.6 W m^{-2} for LHF and 2.6 W m^{-2} for SHF.

The plot of the LHF + SHF differences between 2008 and 2007 (Fig. 3.8b) shows that LHF + SHF had significant changes in the tropical Pacific and Indian Oceans. Positive anomalies are observed in the equatorial eastern Pacific and central tropical Indian Oceans, while negative anomalies are found in the central tropical Pacific. These changes appear to result from the direct response of LHF to SST. The equatorial Pacific in the second half of 2008 was in